

Rectangular prism pressure coherence by modified Morlet continuous wavelet transform

Thai-Hoa Le^{1,2a} and Luca Caracoglia^{*1}

¹Department of Civil and Environmental Engineering, Northeastern University,
360 Huntington Ave., Boston, MA 02115, USA

²Department of Engineering Mechanics and Automation, Vietnam National University, Hanoi,
144 Xuanthuy Rd., Hanoi, Vietnam

(Received September 20, 2014, Revised January 27, 2015, Accepted March 19, 2015)

Abstract. This study investigates the use of time-frequency coherence analysis for detecting and evaluating coherent “structures” of surface pressures and wind turbulence components, simultaneously on the time-frequency plane. The continuous wavelet transform-based coherence is employed in this time-frequency examination since it enables multi-resolution analysis of non-stationary signals. The wavelet coherence quantity is used to identify highly coherent “events” and the “coherent structure” of both wind turbulence components and surface pressures on rectangular prisms, which are measured experimentally. The study also examines, by proposing a “modified” complex Morlet wavelet function, the influence of the time-frequency resolution and wavelet parameters (i.e., central frequency and bandwidth) on the wavelet coherence of the surface pressures. It is found that the time-frequency resolution may significantly affect the accuracy of the time-frequency coherence; the selection of the central frequency in the modified complex Morlet wavelet is the key parameter for the time-frequency resolution analysis. Furthermore, the concepts of time-averaged wavelet coherence and wavelet coherence ridge are used to better investigate the time-frequency coherence, the coherently dominant events and the time-varying coherence distribution. Experimental data derived from physical measurements of turbulent flow and surface pressures on rectangular prisms with slenderness ratios $B/D=1:1$ and $B/D=5:1$, are analyzed.

Keywords: bluff body; time-frequency analysis; turbulence; pressure distribution; flow separation/attachment/reattachment

1. Introduction

Evaluation of the spatial correlation is crucial for an accurate modeling of random forces and buffeting response structural analysis under turbulent wind flows. Conventionally, a Fourier transform-based coherence function has been predominantly employed for representing and modeling the spatial correlation between two random processes (e.g., wind turbulence, pressures and forces) in spatially-correlated random fields. Physically-measured and empirically-based models of the Fourier coherence (e.g., Davenport 1962) have been utilized to adequately describe

*Corresponding author, Associate Professor, E-mail: lucac@coe.neu.edu

^a Visiting Assistant Professor, E-mail: ho.le@neu.edu

the effect of turbulence-induced buffeting loads. Classically, a series of empirical formulae have been directly interpolated from the measurements of wind turbulence, instead of pressures or force fields (more difficult to evaluate experimentally). In these formulae the coherence function is described as an exponential function depending on mean wind velocity, relative distance between the measurement points, frequency, and “gain” or decay factor. Some authors (e.g., Krenk 1996) have questioned the form of the coherence function for turbulence, which can lead to inconsistencies such as a full correlation at very low frequencies, irrespective of distance, and non-zero turbulence fluctuations on the plane transverse to the mean flow direction. The Fourier coherence of pressures has been experimentally studied by some authors (e.g., Larose 1996, Jakobsen 1997). It has also been pointed out (e.g., Matsumoto *et al.* 2003) that the parameters of the Fourier coherence, based on the measurements of pressures or forces, can be larger than the ones obtained from the wind turbulence, which are often employed in the empirical coherence models of the buffeting forces. Furthermore, the Fourier coherence, which indirectly implies averaging of the signals in time and frequency, is applicable to analyze linear and stationary turbulence or pressure “signals”. However, it cannot be used to investigate nonstationary and irregular signals, for example in cases of non-synoptic and extreme wind events (Bruns 2004, Zhan *et al.* 2006) or nonlinear fluid-structure interaction. More importantly, the Fourier coherence cannot reveal localized high coherence, time-varying and intermittent coherent flow and pressure “features”. Also no temporal information can be provided in the Fourier coherence.

In order to overcome these limitations, a “wavelet transform-based coherence” analysis is considered in this study for investigating the correlation of both wind turbulence and surface pressures simultaneously on the time-frequency plane. The wavelet coherence can detect the localized high-coherence “events” and explore the time-frequency coherent structures in a non stationary random field. Torrence and Compo (1998) first introduced the use of the wavelet coherence for the correlation of meteorological data. Geurts *et al.* (1998) employed the concept of “cross” wavelet transform coefficients to detect the cross correlation between measured wind turbulence and pressures on full-scale low-rise buildings. The wavelet coherence analysis has been extensively used to examine the cross correlation and the time-frequency coherence of various kinds of measured stationary and nonstationary signals. Examples are: turbulence and pressure measurements (e.g., Kareem and Kijewski 2002, Gurley *et al.* 2003, Le *et al.* 2009); geophysical signals (Grinsted *et al.* 2004); meteorological signals (Torrence and Compo 1998); electrophysiological signals (e.g., Bruns 2004, Zhan *et al.* 2006). Le *et al.* (2009, 2011) examined the pressure coherence on rectangular prisms with different slenderness ratios $B/D=1:1$, $B/D=5:1$ using the wavelet transform and a coherence analysis approach, based on the proper orthogonal decomposition. The same study also focused on the influence of the spanwise separation, the bluff body flows on the model’s surface, the Karman vortices in the wake, the intermittency features and the coherent “structures” of wind turbulences and surface pressures. The main findings of these studies can be summarized as (Le *et al.* 2009, 2011): (i) coherent pressure structures not only depend on the frequency, the distance, and the mean flow velocity (as in Davenport’s model), but also on the turbulent conditions and the bluff body flow; (ii) dominant physical phenomena originating from the model “signature” and in the wake can significantly influence the coherent structure; (iii) intermittent and locally-distributed high coherence is exhibited by the coherence structures on the time-frequency plane; and (iv) pressure coherence can be considerably larger than the turbulence coherence. In the case of wake structures around rectangular prisms, Bruno *et al.* (2014) recently discussed the status of an ongoing benchmark study on the aerodynamic behavior of a prism with slenderness $B/D=5:1$. A series of studies by five distinct research groups, including

wind tunnel experimental results and several investigations by computational simulations (CFD) were discussed. It is found that the magnitude of the spanwise pressure correlation coefficients for this prism can vary considerably from data set to data set, and that spanwise pressure correlation is usually stronger in the region of the separation “bubble”, immediately beyond the flow separation point. However, Bruno *et al.* (2014) remarked the inherent difficulty in identifying a reference experiment or simulation that enables efficient benchmark comparison for each designated flow configuration. Furthermore, high sensitivity of flow configurations (e.g., flow speed and turbulence intensity) on the spatial distribution of the spanwise pressure correlation magnitudes was also observed. In any case, information on chordwise pressure correlation and chordwise coherence has not been reported in Bruno *et al.* (2014).

It is generally agreed that computations of the wavelet transform and the wavelet coherence are actually complex and time-consuming. Basic parameters of the “mother” wavelet function can significantly affect the wavelet coherence analysis; in particular, scale normalization, time-scale smoothing and time-frequency resolution analysis are required in computing the wavelet transform and the wavelet coherence (Torrence and Compo 1998). However, rare comprehensive studies exist on the influence of time-frequency resolution and time-scale smoothing on the accuracy of the wavelet coherence estimation. In wind engineering, the continuous Morlet wavelet has been traditionally employed (e.g., Kareem and Kijewski 2002, Le *et al.* 2011). Moreover, the spanwise coherence of the surface pressures has been exclusively investigated (Le *et al.* 2009, 2011). The influence of the time-frequency resolution and adequate selection of a wavelet function, which is more adaptable to the needs of the multi-resolution analysis, still require examination. Furthermore, time-scale smoothing and scale normalization are needed for the wavelet-transform-based quantities; otherwise, the wavelet coherence can be incorrectly estimated as identically one (i.e., full correlation) on the time-scale plane (e.g., Li 2004, Kareem and Kijewski 2002).

This study builds on the existing literature results and systematically explores time-frequency continuous wavelet transform-based coherence function to examine the coherent structures of the surface pressures on rectangular prisms. The surface pressure data have been derived from a series of rigid section-model wind tunnel experiments (Matsumoto *et al.* 2003, Le *et al.* 2009) in the turbulent flows on rectangular prisms with various slenderness ratios $B/D=1:1$, $B/D=1:1$ with a splitter plate (SP) and $B/D=5:1$. The main objectives of the study are to:

- (1) Investigate the influence of time-frequency resolution on the estimation of time-frequency pressure coherence function;
- (2) Examine the use of a “modified” complex continuous Morlet wavelet, which can easily be adapted to various time-frequency resolution ranges and time-scale smoothing intervals;
- (3) Evaluate intermittency of surface pressures through the new concepts of time-averaged coherence and coherence ridge.

2. Fourier coherence - definitions

The Fourier coherence between two zero-mean random processes $X(t)$ and $Y(t)$ in a spatially-correlated random field can be determined by normalization of correlation coefficients of the two spectral quantities of vector signals $X(t)$ and $Y(t)$ in the frequency domain (Bendat and Piersol 2000)

$$COH_{XY}^2(f) = \frac{|S_{XY}(f)|}{\sqrt{S_X(f)S_Y(f)}} \quad (1)$$

where $|\cdot|$ denotes absolute operator; f : Fourier frequency variable; $S_X(f), S_Y(f), S_{XY}(f)$: Fourier auto power spectra and Fourier cross power spectrum at/between two separated points, respectively as

$$S_X(f) = E[\hat{X}(f)\hat{X}(f)^{*T}]; S_Y(f) = E[\hat{Y}(f)\hat{Y}(f)^{*T}]; S_{XY}(f) = E[\hat{X}(f)\hat{Y}(f)^{*T}] \quad (2)$$

where $E[\cdot]$ is the expectation operator; it is noted that the limit and time averaging operations (Bendat and Piersol 2000) have been omitted in the notation of Eqs. (2) for simplicity. Besides, the superscript symbols “*”, “ T ” denote complex conjugate and transpose operators; $\hat{X}(f), \hat{Y}(f)$ are the Fourier transforms of $X(t), Y(t)$ respectively with f frequency. The Fourier coherence is normalized between 0 and 1. It is known that if the random processes $X(t)$ and $Y(t)$ are fully-correlated, the Fourier coherence is one, whereas the Fourier coherence is zero if the two processes are uncorrelated.

3. Wavelet coherence

3.1 Definitions

Continuous wavelet transform (CWT) of random process $X(t)$ is defined as the convolution operation between $X(t)$ and the “mother” wavelet function $\psi_{\tau,s}(t)$ (Daubechies 1992)

$$W_X^\psi(\tau, s) = \int_{-\infty}^{\infty} X(t)\psi_{\tau,s}^*(t)dt \quad (3)$$

where the quantity $W_X^\psi(\tau, s)$ contains the wavelet transform coefficients at translation index “ τ ” and scale index “ s ” on the time-frequency plane; the superscript “*” denotes complex conjugate; $\psi_{\tau,s}(t)$ is the dilated and translated wavelet function of the “mother” wavelet $\psi(t)$ at translation τ and scale s . The dilated and translated $\psi_{\tau,s}(t)$ is estimated as

$$\psi_{\tau,s}(t) = \frac{1}{\sqrt{s}}\psi\left(\frac{t-\tau}{s}\right) \quad (4)$$

The wavelet transform coefficients $W_X^\psi(\tau, s)$ can be considered as a correlation coefficient and a measure of similitude between the wavelet function and the original process in the time-scale plane. The CWT of a discrete series X_i ($i=0, \dots, N-1$) can be expressed as $W_{X_i}(s) = \sum_{i'=0}^{N-1} X_{i'}\psi^*[(i'-i)\delta t/s]$, in which $W_{X_i}(s)$ are the continuous wavelet coefficients at the discrete time point i and δt is a time interval (depending on the digitalization of the signal).

3.2 From the complex Morlet wavelet to the modified Morlet wavelet

The basic Morlet wavelet is predominantly used in the CWT since it contains a harmonic component, analogous to the Fourier transform, which is better suited to capture oscillatory behavior in a random process (Kareem and Kijewski 2002, Gurley *et al.* 2003)

$$\psi(t) = (2\pi)^{-1/2} \exp(i2\pi f_c t) \exp(-t^2 / 2) \tag{5}$$

where f_c denotes the wavelet central frequency, which can be taken as equal to one in many simplified cases. The basic Morlet wavelet is a complex harmonic function.

Nevertheless, the exclusive dependency on one parameter, i.e., the central frequency f_c , does not seem to be sufficient for simultaneously analyzing multiple time-frequency resolution “scales”. Therefore, a modified form of the basic complex Morlet wavelet is applied in this study to enable a more “flexible” analysis of the time-frequency resolution

$$\psi(t) = (\pi f_b)^{-1/2} \exp(i2\pi f_c t) \exp(-t^2 / f_b) \tag{6}$$

where f_b is a bandwidth parameter (Yan *et al.* 2006). A fixed bandwidth parameter is often used, $f_b=2$, in the traditional Morlet wavelet. The basic complex Morlet wavelet is only a special case of the modified complex Morlet wavelet with bandwidth parameter $f_b=2$. The modified complex Morlet wavelet satisfies the admissibility condition and the convergence of the corresponding integral (Daubechies 1992). Similar to the basic Morlet wavelet, the modified complex Morlet wavelet possesses the features of non-orthogonality, complex harmonic-type function and multi-resolution adaptation. Generally, the central frequency is related to the number of waveforms in the wavelet window, whereas the bandwidth parameter regulates the width of the wavelet window. Time-frequency resolution of the Morlet wavelet in Eq. (6) is determined by the balance between the width of the window in the real time axis and the number of waveforms. For example, a narrow window in time has a good time resolution but poor frequency resolution, while a broad window has a poor time resolution but good frequency resolution.

3.3 Wavelet coherence

For two random processes $X(t)$ and $Y(t)$, wavelet transform-based auto spectrum, wavelet cross spectrum, wavelet cross spectrum at time shift of index “ τ ” and the scale “ s ” can be defined from the respective wavelet transform coefficients $W_{X_i}(s)$ and $W_{Y_i}(s)$ as (Bruns 2004, Zhan 2006)

$$WPS_{XX_i}(s) = \langle W_{X_i}(s)W_{X_i}^{*T}(s) \rangle; WPS_{YY_i}(s) = \langle W_{Y_i}(s)W_{Y_i}^{*T}(s) \rangle; WCS_{XY_i}(s) = \langle W_{X_i}(s)W_{Y_i}^{*T}(s) \rangle \tag{7}$$

where $WPS_{XX_i}(s)$, $WPS_{YY_i}(s)$ are wavelet auto spectra of $X(t)$, $Y(t)$; $WCS_{XY_i}(s)$ is the wavelet cross spectrum between $X(t)$ and $Y(t)$; the symbol $\langle \cdot \rangle$ denotes “smoothing operator” on both time and scale axes. The time-scale smoothing is a local-averaging signal processing technique of the wavelet window in the time and the scale (frequency).

Similar to the Fourier coherence, the squared wavelet coherence of $X(t)$ and $Y(t)$ can be defined as the squared value of the absolute smoothed wavelet cross spectrum, normalized by the smoothed wavelet auto spectra (Torrence and Compo 1998)

$$WCO_{XY}^2(s) = \frac{|\langle s^{-1}WCS_{XY}(s) \rangle|^2}{\langle s^{-1} | WPS_{XX}(s) | \rangle \langle s^{-1} | WPS_{YY}(s) | \rangle} \quad (8)$$

where $WCO_{XY}(s)$ is the wavelet coherence of $X(t)$ and $Y(t)$. Normalization is used in the previous equation to satisfy the requirement of unitary energy density at any scale. Since the dilated wavelet is defined by the factor \sqrt{s} in Eq. (4), a term s^{-1} has been added to the wavelet coherence in Eq. (8). The scale normalization ensures that the wavelet transforms of the process at each scale are compatible with transforms at another scale or those of other process.

Furthermore, wavelet phase difference can be estimated from the wavelet cross spectrum as

$$WPD_{XY}(s) = \tan^{-1} \frac{\text{Im} \langle s^{-1}WCS_{XY}(s) \rangle}{\text{Re} \langle s^{-1}WCS_{XY}(s) \rangle} \quad (9)$$

Numerical estimation of wavelet transform and wavelet coherence can be inaccurate if the scale normalization and time-scale smoothing are not taken into account, as described in a later section of this study.

3.4 Scale and frequency relationship

The wavelet transform employs the scale parameters, which is the inverse of a frequency. A relationship between the wavelet scale and the Fourier frequency can be obtained

$$s = \frac{f_c}{f} \quad (10)$$

Eq. (10) is valid if a unit sampling frequency of the wavelet function is used. Practically, the sampling frequency of a random signal must be included in the scale-frequency relationship as (e.g., Staszewski 1998, Le *et al.* 2009)

$$s = \frac{f_0 f_c}{f} \quad (11)$$

in which f_0 denotes the sampling frequency of the random process $X(t)$.

3.5 Time-scale smoothing

Smoothing in both time and scale is necessary for estimating high-order wavelet transform-based quantities such as the wavelet auto spectra, the wavelet cross spectra, the wavelet coherence and the wavelet phase difference. The main purpose of the smoothing is to obtain a more accurate “estimator” of the wavelet transform by removing noise and by converting the estimated quantity from a “local” wavelet power spectrum to a “global” wavelet power spectrum. Similar to the Fourier transform-based power spectrum, in the case of a smoothing in time, the time-averaged wavelet power spectra can be computed either over a discrete time interval $[i_1, i_2]$,

referenced to a time-shifted index $i'=(i_1+i_2)/2$, or over the entire time domain (Torrence and Compo 1998)

$$\langle WPS_{i'}^2(s) \rangle = 1 / (i_2 - i_1 + 1) \sum_{i=i_1}^{i_2} |WPS_i(s)|^2 \tag{12a}$$

$$\langle WPS_N^2(s) \rangle = 1 / N \sum_{i=0}^{N-1} |WPS_i(s)|^2 \tag{12b}$$

In the previous equations i_1 and i_2 are two indices used to designate the initial time and final time of the smoothing period; N is the number of sampled points in the entire time domain. In this study, the smoothing in time over the entire time domain in Eq. (12(b)) has been employed for comparison with the Fourier transform-based coherence.

In the case of a smoothing in scale, a weighted scaled-averaged wavelet power spectrum over a scale range between s_1 and s_2 has been proposed by Torrence and Compo (1998)

$$\langle WPS_i^2(s) \rangle = \frac{\delta t \delta j}{C_\delta} \sum_{j=j_1}^{j_2} \frac{|WPS_i(s_j)|^2}{s_j} \tag{13}$$

where j is a scaling index between j_1 and j_2 ; δt is the time interval; δj is a scale interval; C_δ is a constant empirical reconstruction factor of the Morlet wavelet, scale independent. The C_δ factor is determined (Torrence and Compo 1998) as $C_\delta = (\delta_j \delta_t^{1/2} / \psi_0(0)) \sum_{j=0}^J Re[W_\delta(s_j)] / s_j^{1/2}$, where $\psi_0(0)$ is the mother Morlet wavelet at the initial time $t=0$ at the initial scale $s \approx 0$; $W_\delta(s_j)$ is CWT coefficient of the delta function δ ; Re denotes real part of the operator. Further information on the time-scale smoothing may be found in Torrence and Compo (1998).

3.6 End-effect treatment

Because the wavelet function with a finite window width is applied to a finite-duration random process, a loss of accuracy will occur at the beginning and the end of the wavelet spectrum. This is also known as the end effect or “cone of influence” or “padding effect” of the wavelet transform. The cone of influence depends on the scale (the frequency). Concretely, the cone of influence is wider at low frequency and narrower at high frequency. One simple solution to deal with the end effects of the wavelet spectrum is to first pad the two ends of the random signal with zeroes before the wavelet spectrum is computed, and to subsequently remove the wavelet coefficients corresponding to the zero-padded time instants. Padding at the two ends of the wavelet spectrum has been proposed by applying a reduction factor e^{-2} to the scale values at the two ends of the spectrum (Torrence and Compo 1998, Grinsted *et al.* 2004). In this study, a simplified treatment of the end effects has been chosen, by eliminating 5-second intervals of the numerically estimated wavelet spectrum at the two ends. More sophisticated approaches (e.g., Simonovski and Boltežar 2003, Kijewski and Kareem 2002) are available for managing the evaluation of the wavelet spectrum at two ends of a signal recorded over a finite time duration.

3.7 Time-frequency resolution

The wavelet coherence is the basis of the multi-resolution analysis. Time-frequency resolution is examined by simultaneously considering the frequency and wavelet function parameters. However, the uncertainty principle of the wavelet analysis states that, since the product of frequency response scale and time resolution has a lower bound, it is not possible to simultaneously achieve optimal time and frequency resolutions (e.g., Ladies and Gouttebroze 2002, Kijewski and Kareem 2002). A fine frequency resolution implies a coarse time resolution, and inversely coarse frequency resolution comes with a fine time resolution. Fortunately, in many practical signals the fine frequency resolution and the coarse time resolution are often employed for analyzing low frequency band.

The time-frequency resolution for the wavelet coherence using the traditional Morlet wavelet function with the central frequency equal to one can be expressed, in the optimal relationship, as (Kijewski and Kareem 2003)

$$\Delta f_{\psi} = \frac{1}{2\pi\sqrt{2}}, \Delta t_{\psi} = \frac{1}{\sqrt{2}} \quad (14)$$

where Δf_{ψ} and Δt_{ψ} are frequency resolution and time resolution of the Morlet wavelet. The optimal product between the frequency resolution and the time resolutions is $\Delta f_{\psi}\Delta t_{\psi} = 1/4\pi$. Normally, we have the relationship $\Delta f_{\psi}\Delta t_{\psi} \geq 1/4\pi$. The time-frequency resolution relationships of the traditional Morlet wavelet, with central frequency parameter $f_c \neq 1$, at a given frequency f , become (Yan *et al.* 2006)

$$\Delta f = \frac{\Delta f_{\psi}}{s} = \frac{f}{2\pi f_c \sqrt{2}}, \quad \Delta t = s\Delta t_{\psi} = \frac{f_c}{f\sqrt{2}} \quad (15)$$

In this study, the definition of time-frequency resolution can be further extended by accounting for the presence of the bandwidth parameter f_b as follows

$$\Delta f = \frac{f}{2\pi f_c \sqrt{f_b}}, \quad \Delta t = \frac{f_c}{f\sqrt{f_b}} \quad (16)$$

Table 1 illustrates the time-frequency resolution of the modified Morlet wavelet for various combinations of the central frequency (f_c) and the bandwidth parameter (f_b), as a function of the analyzed frequencies (f). As evident from Table 1, the complex Morlet wavelets possess the fine frequency resolution and the coarse time resolution at the lower analyzing frequencies, and inversely the coarse frequency resolution and the fine time resolution at the higher analyzing frequencies. This scenario is expected in the practical signals. According to Table 1, the frequency resolution is finer and the time resolution is coarser with the progressive increment of the central frequency f_c and the bandwidth parameter f_b . Therefore, one can adjust the wavelet central frequency f_c and the bandwidth parameter f_b to obtain both desired frequency and time resolutions, depending on the analyzed frequency.

Fig. 1 indicates the real and imaginary parts of various examples of modified complex Morlet wavelets. It is observed that, at a constant f_c and for an increasing f_b , the time-window width is enlarged but the wavelet “shape” and the magnitude of the spectral peaks in the wavelets are

unchanged. In contrast, at a constant f_b the number of waveforms considerably increases with the increment of f_c . The efficient numerical computation of the wavelet coherence is, consequently, negatively affected by the increase in the number of waveforms. Therefore, it is desirable to keep the central frequency f_c as low as possible ($f_c=1, 2$) and increase the bandwidth parameter f_b to fit with desired time-frequency resolution at the analyzing frequencies.

3.8 Confidence intervals

Confidence interval of a wavelet quantity is defined as the probability that the “true” value of the wavelet quantity, at a certain time and scale, lies within a certain interval of the estimated value of the quantity. Since the wavelet spectrum, the wavelet cross spectrum, the wavelet coherence and the wavelet phase difference are estimated from random pressure data by manipulating the signals the statistical confidence levels of the resulting wavelet quantities need to be assessed. As described by Torrence and Compo (1998), the confidence is examined by the “null hypothesis” on the statistical significance level, which requires the initial derivation of an appropriate background power spectrum. The simplest models of background power spectrum are the white noise and the “red noise” (Torrence and Compo 1998). These two spectral models are applied, as a first approximation, to investigate the wind-induced surface pressures in this study. In particular, the red noise of a random process $X(t)$ is modelled as a first-order autoregressive process (AR1) to build up a suitable background Fourier power spectrum (Torrence and Compo 1988)

$$P_k^X = \frac{1-\alpha^2}{1+\alpha^2-2\alpha\cos(2\pi k/N)} \tag{17}$$

In the previous equation P_k^X denotes the power spectrum of X ; α is the lag-1 autocorrelation of the AR1 model; $k=0,1,\dots,N/2$ is the frequency index. It is noted that the lag-1 autocorrelation α can be determined from the measured pressures; $\alpha = 0$ can be used for white noise.

The random normalized wavelet spectrum $|WPS_{XX,i}|/\sigma_X^2$, and the wavelet cross spectrum $|WCS_{XY,i}|/\sigma_X \sigma_Y$ of the pressure time series X and Y , with a background power spectrum as in Eq. (17), can be written as two standard distribution variables (Torrence and Compo 1998)

$$\frac{|WPS_{XX,i}|}{\sigma_X^2} \sim \frac{1}{2} P_k^X \chi_\nu^2 \tag{18a}$$

$$\frac{|WCS_{XY,i}|}{\sigma_X \sigma_Y} \sim \frac{Z_\nu}{\nu} \sqrt{P_k^X P_k^Y} \tag{18b}$$

where σ_X^2, σ_Y^2 are the variances of the original time series; χ_ν^2 is the chi-square random variable distribution with ν degrees of freedom (χ_2^2 for the complex wavelets, $\nu = 2$); P_k^X, P_k^Y are the background power spectra; Z_ν is a random variable defined by the square root of the product between two chi-square distributions. The confidence intervals can be found from Eqs. (18) as indicated in Torrence and Compo (1998).

Since the probability distribution of the wavelet coherence is not usually available in closed form, confidence levels of the wavelet cross-coherence are typically estimated by Monte Carlo simulation (Grinsted *et al.* 2004) as follows: (i) estimate the wavelet coherence (and cross-coherence) of the measured pressures at X and Y ; (ii) generate a suitable sample of red noise realizations based on the AR1 model parameters derived from the original pressures; (iii) compute the wavelet coherence from two pairs of simulated red noises with background Fourier spectrum

P_k^X, P_k^Y ; (iv) estimate the margins of error of the wavelet coherence corresponding to a pre-selected confidence interval from the red-noise population; (v) determine the confidence intervals of the true wavelet coherence based on the measured wavelet pressure coherence and the error margins in item (iv).

Table 1 Time and frequency resolutions of wavelet parameters at selected frequencies

Analyzed freq. (f)	5Hz		10Hz		20Hz		30Hz	
Time-frequency Resolution	Δf (Hz)	Δt (s)						
$f_c=1, f_b=2$	1.25	0.14	2.50	0.07	5.00	0.04	7.50	0.02
$f_c=1, f_b=5$	0.79	0.22	1.58	0.11	3.16	0.06	4.74	0.04
$f_c=5, f_b=2$	0.25	0.71	0.50	0.35	1.00	0.18	1.50	0.12
$f_c=5, f_b=5$	0.16	1.12	0.32	0.56	0.63	0.28	0.95	0.19
$f_c=10, f_b=2$	0.13	1.41	0.25	0.71	0.50	0.35	0.75	0.24
$f_c=10, f_b=5$	0.08	2.24	0.16	1.12	0.32	0.56	0.47	0.37

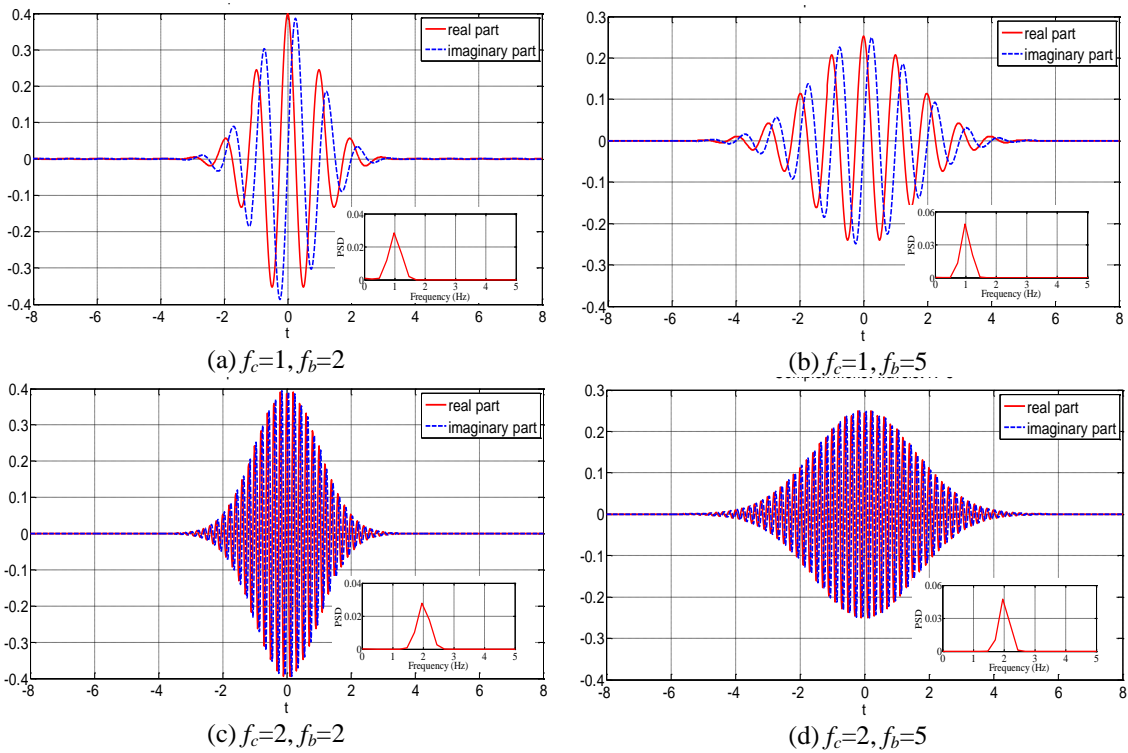


Fig. 1 Configuration of modified complex Morlet wavelets: (a) $f_c=1, f_b=2$, (b) $f_c=1, f_b=5$, (c) $f_c=2, f_b=2$, (d) $f_c=2, f_b=5$

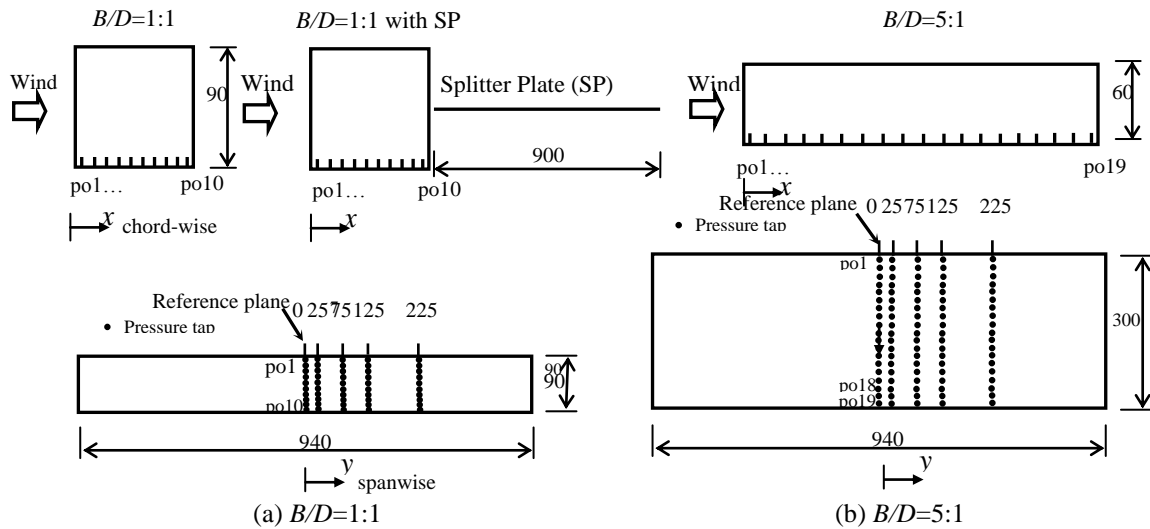


Fig. 2 Experimental prisms and surface pressure measurement: (a) $B/D=1:1$ and (b) $B/D=5:1$

4. Surface pressures on prisms

Surface pressure signals were derived from direct measurements on the rectangular prisms with the slenderness ratios of $B/D=1:1$, $B/D=1:1$ with SP and $B/D=5:1$ in the wind tunnel (Le *et al.* 2009, 2011). Isotropic turbulent flows were generated artificially using grid devices, installed upstream of the prisms. The two-component fluctuating wind velocities (longitudinal u turbulence and vertical w turbulence) were also measured. Turbulence intensities of these two components were determined as $I_u=11.56\%$, $I_w=11.23\%$, respectively. Pressure taps were arranged on one surface of the prisms for the surface pressure measurements. There were 10 pressure tap “lines” on the prism with $B/D=1:1$ and 19 pressure taps on the prism with $B/D=5:1$ in the chordwise direction; the separations among pressure tap lines in the spanwise direction from the reference line at $y=0$ mm (central line) were selected at the positions $y=25, 75, 125$ and 225 mm (Fig. 2).

5. Results and discussion

Fig. 3 shows the spanwise wavelet coherences of the w -wind turbulence and the surface pressures on the prisms at the spanwise separations between the reference point at $y=0$ and $y=25$ mm ($y/B=0.27$ in $B/D=1:1$, $y/B=0.08$ in $B/D=5:1$, see Fig. 2) in the frequency interval between 0 and 50 Hz and time interval between 5 and 95 seconds. In this study, normalization in scale and smoothing in time and scale have been applied for computation of the wavelet coherence. As outlined above, 5-second intervals at the beginning and the end of the computed wavelet coherence have been eliminated to deal with the loss of accuracy and the end effects. The wavelet coherence can be used to illustrate “coherent events” in both turbulence and surface

pressures at every point on the time-frequency plane. Different shades of color are used in the wavelet coherence maps: lighter colors indicate a coherence value close to the unit value, whereas darker colors are used for coherence close to zero.

The wavelet coherence detects any localized high-coherence events at a specific frequency or bandwidth and at a given time or duration. Clearly, more information can be obtained from the wavelet coherence in comparison with the Fourier coherence. It is also observed that the pressure (auto) coherence gradually decreases as the slenderness ratio of the prisms increases, from $B/D=1:1$, the $B/D=1:1$ with SP to the $B/D=5:1$, respectively. The pressure coherence on the prisms is much larger than the vertical turbulence coherence. High-coherence events of the pressures are not coincident with wind turbulence coherence data on the time-frequency plane.

For example, if one examines the time evolution of pressure coherence in Fig. 3(c) at a frequency close to 2 Hz, the pressure coherence is large and intermittent, also suggesting a temporal dependency of the unsteady pressure “features or structures”. In contrast, the same feature is not evident from the analysis of the wavelet spectrogram of the w turbulence component in Fig. 3(d) at the same frequency. The difference in the wavelet coherence, measured on the different prisms and a larger pressure coherence in comparison with flow turbulence confirm the effect of bluff body flow on the coherent structures of the pressures.

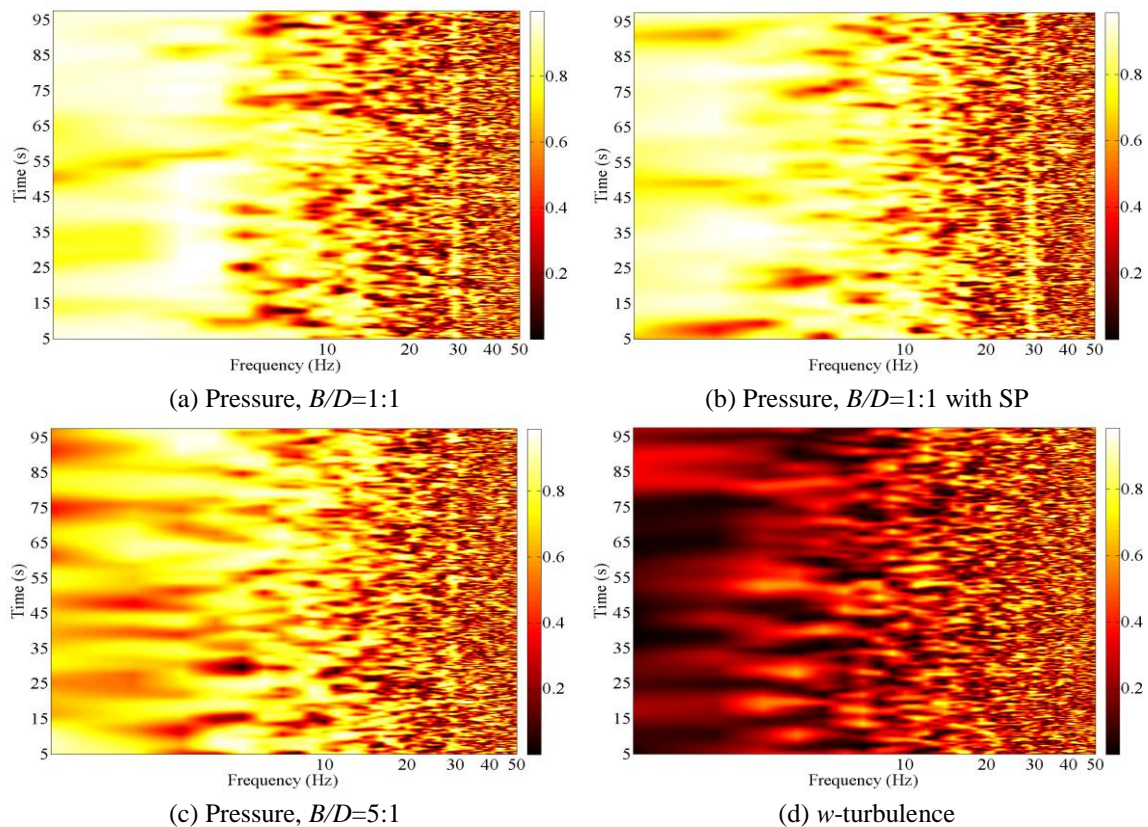


Fig. 3 Spanwise wavelet coherence: (a) $B/D=1:1$, (b) $B/D=1:1$ with SP, (c) $B/D=5:1$, (d) w -turbulence

Similar to the spanwise coherence, the chordwise coherence of the surface pressure has been investigated. Fig. 4 illustrates the chordwise wavelet coherences of the pressures on the prisms at the chordwise separations between the reference point at $x=0$ and $x=25$ mm, measured at the bottom surface of the prism. The chordwise pressure coherence “structure” is also observed on the time-frequency plane, similar to the spanwise coherence structure. However, the chordwise pressure coherence seems to be stronger than the spanwise coherence (see Figs. 3 and 4).

For more detailed investigation on the time-frequency coherence, the concepts of time-averaged wavelet coherence and wavelet coherence ridge are employed. Fig. 5 illustrates how to estimate these quantities from the wavelet coherence scalogram. The averaged wavelet coherence is obtained by averaging the wavelet coherence along the entire time axis (95-second signal duration). As a result, the averaged wavelet coherence can be approximately interpreted as a quantity similar to the Fourier coherence in the frequency domain. In addition, the wavelet coherence ridge can be found by inspection, using vertical-plane cross sections in the wavelet coherence scalogram along the time axis at constant frequency, which coincide with the peak value of the wavelet coherence. Thus, the wavelet coherence ridge provides further information about intermittent behavior of pressures or flow. In Fig. 5 the averaged wavelet coherence is a frequency-dependent function, whereas the wavelet coherence ridge is a time-dependent one.

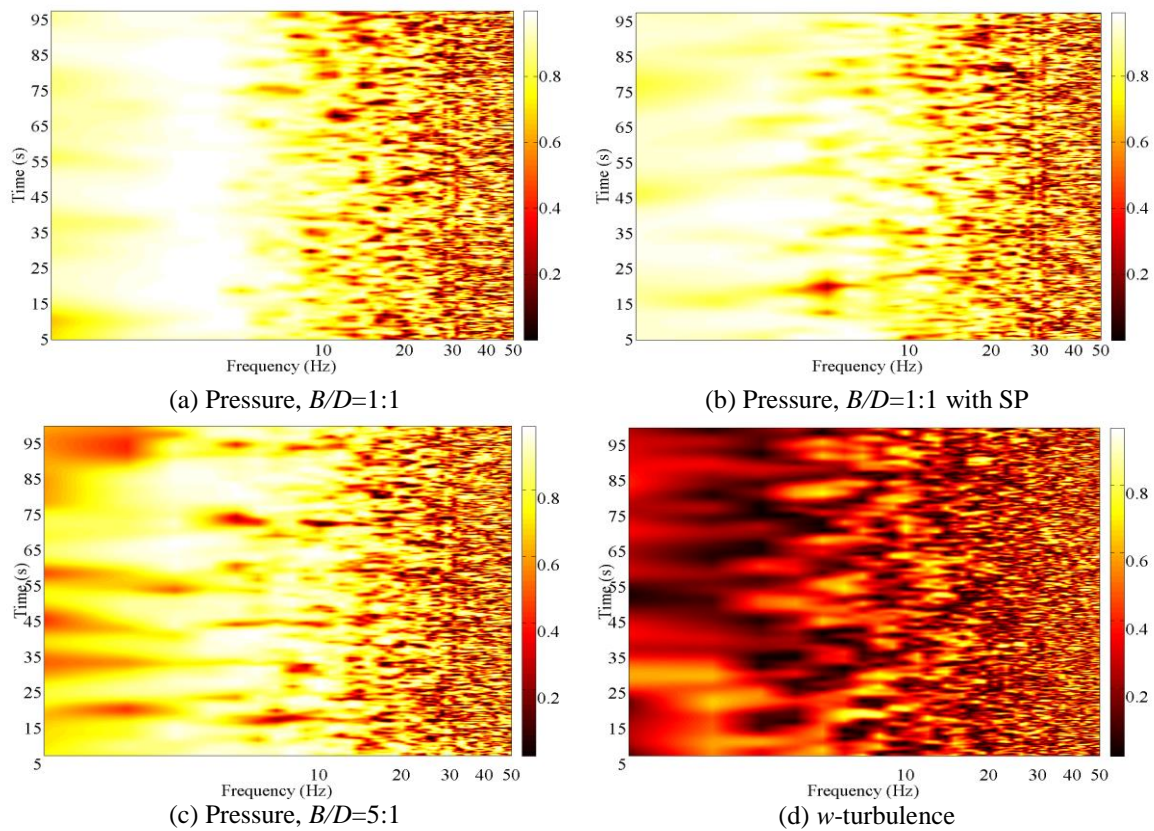


Fig. 4 Chordwise wavelet coherence: (a) $B/D=1:1$, (b) $B/D=1:1$ with SP, (c) $B/D=5:1$

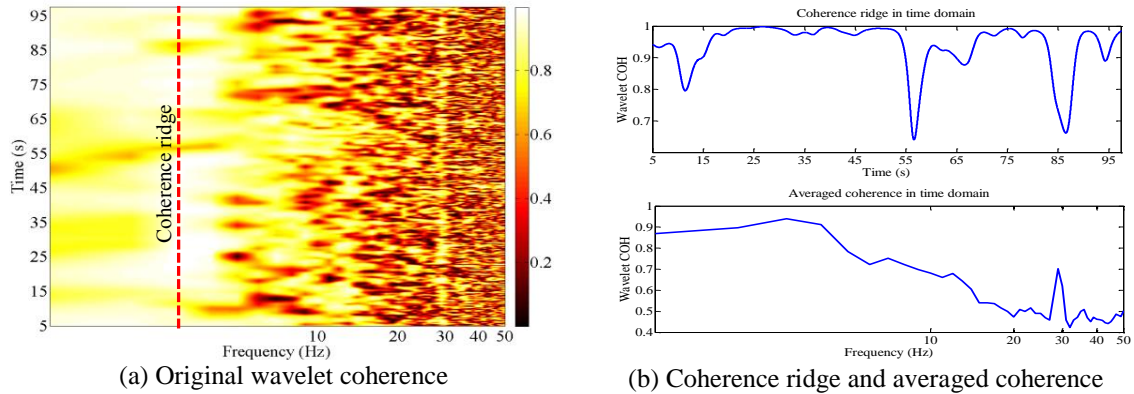


Fig. 5 Mapping of wavelet coherence function: (a) Original wavelet coherence, (b) Coherence ridge and averaged coherence

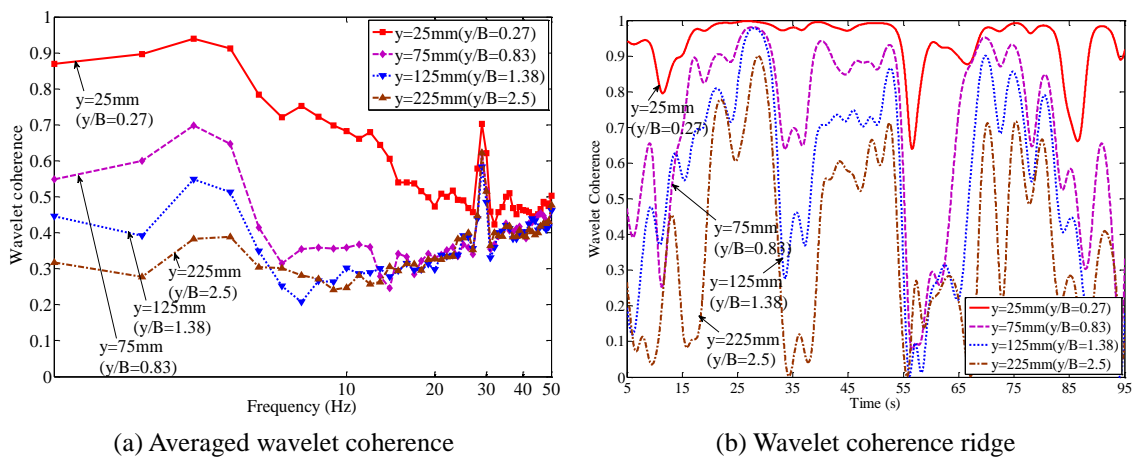


Fig. 6 Wavelet coherence of pressures at various spanwise separations ($B/D=1:1$): (a) Averaged wavelet coherences, (b) Wavelet coherence ridges

Fig. 6 shows the averaged wavelet coherence and the wavelet coherence ridges of the pressures on the $B/D=1:1$ prism at the spanwise separations between the reference point at $y=0$ and $y=25, 75, 125$ and 225 mm. It is noted in Fig. 6(a) that the averaged wavelet coherence decreases with the increment of the spanwise separations. However, the averaged wavelet coherence of the pressures does not seem to exhibit fast decay at high frequency. High-coherence regions at about 5 Hz are also clearly observed in the averaged wavelet coherence diagrams, in correspondence with the frequency of Karman vortices in the wake of the prisms with $B/D=1:1$. Locally, low and high coherence events in the pressures at the dominant frequency are investigated by the wavelet coherence ridge in the time domain. Fig. 6(b) shows that low coherence events and their durations increase with the increment of spanwise separation. Moreover, very low coherence events can be observed at approximately equidistant separations. Interestingly, the wavelet coherence ridges at various spanwise separations reveal a similar shape along the time axis. In other words,

high-coherence events and low-coherence ones seem to occur in the case of pressures at the same times and at almost every spanwise separation (irrespective of the separation distance). For example, high-coherence events approximately occur at 28, 52, 71, 76 and 80 seconds, while low-coherence events are observed at 12, 34, 57, 62, 77 and 86 seconds in the wavelet coherence ridges of the pressure on the $B/D=1:1$ prism (see Fig. 6(b)).

Fig. 7 illustrates the comparisons between averaged wavelet coherence and Fourier coherence for both wind turbulence and surface pressures at the spanwise and chordwise separations between the reference point at $x=0, y=0$ and $x=25\text{ mm}, y=25\text{ mm}$. There is adequate agreement between the wavelet coherence and the Fourier coherence in the low frequency band. However, difference is noted between the two curves in the high frequency band and for the spanwise direction (Fig. 7(a)).

A better agreement between wavelet coherence and Fourier coherence is found along the entire frequency axis in the chordwise direction (Fig. 7(b)). The Fourier coherence seems to decay faster than the wavelet coherence at high frequencies. A reason for this difference is still unknown and will require further investigation. Fig. 7 also examines the “intensity” of the coherent structures of both wind turbulence and pressures, derived from Figs. 3 and 4. The pressure coherence on the $B/D=1:1$ prism is larger than the one on the $B/D=5:1$ in both spanwise and chordwise directions. Pressure coherences on both the $B/D=1:1$ and $B/D=5:1$ prisms are larger than the vertical turbulence coherence. Furthermore, there is a difference in the pressure coherences between the $B/D=1:1$ prism and the $B/D=1:1$ prisms with SP in both spanwise and chordwise directions. It seems that the pressure coherences on the $B/D=1:1$ prism with SP are slightly higher at very low frequencies (less than 5 Hz), whereas pressure coherences on the $B/D=1:1$ prism clearly become predominant around the Karman vortex frequency interval. Effect of a variation in the fundamental flow (e.g., separation and reattachment, vortex structure, bubble, etc.) on the surface of the bluff body prisms explains the differences in the pressure coherences and the turbulence coherence. Fundamental (related to fluid-structure interaction) and secondary flows (related to convection flow mechanisms) on the model surface may enhance or suppress the pressure coherences in the spanwise and chordwise directions (e.g., Matsumoto *et al.* 2003, Le *et al.* 2009). Furthermore, it is observed that the chordwise pressure coherences seem larger than the spanwise pressure coherences on the surface of the same prisms.

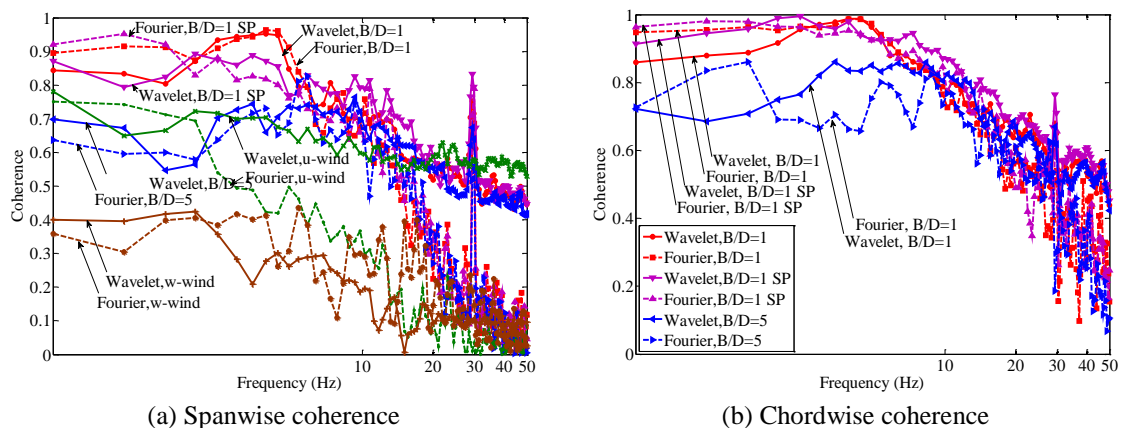


Fig. 7 Comparison between wavelet and Fourier coherences of pressure and turbulence components (u, w): (a) Spanwise coherence, (b) Chordwise coherence

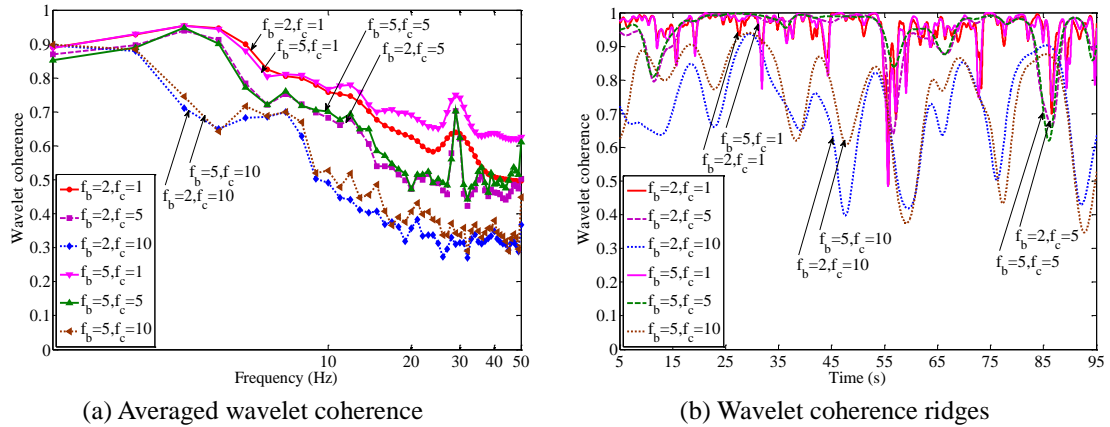


Fig. 8 Effect of time-frequency resolution: (a) Averaged wavelet coherence, (b) Wavelet coherence ridges

The influence of the time-frequency resolution on the time-frequency coherence and, in particular, on the averaged wavelet coherence and the wavelet coherence ridges of the pressures, has been investigated in Fig. 8 for the $B/D=1:1$ prism at the spanwise separation distance equal to 25 mm. An illustration of time-frequency resolution in the case of the modified Morlet wavelet parameters, depending on central frequency f_c and bandwidth parameter f_b , has been provided in Table 1. The time-frequency resolution considerably affects both the averaged wavelet coherence and the wavelet coherence ridges. The averaged wavelet coherence of the pressures on the $B/D=1:1$ prism reduces with an increase of the central frequency f_c , while it does not vary with the bandwidth parameter f_b (Fig. 8(a)). Similar observation on the wavelet coherence ridges can be drawn from Fig. 8(b) by modifying the central frequency f_c and the bandwidth parameter f_b . Identification of intermittent behavior in the wavelet coherence ridges, depending on the selection of the wavelet function parameters, has been examined in Fig. 8(b). Higher intermittency rate with sudden low coherence events is frequently observed if the central frequency f_c is high. It also seems that low- and high-coherence events occur at approximately the same time instants along the time axis if the same central frequency is used.

The main remarks of this examination are: (i) wavelet central frequency f_c is the key parameter for adequate time-frequency analysis; (ii) time resolution decreases but frequency resolution increases with the increase of the wavelet central frequency f_c ; (iii) the bandwidth parameter f_b is a correction parameter in the time-frequency resolution analysis; and (iv) frequency resolution increases but time resolution decreases with the increase of the bandwidth parameter f_b . It is advised to select a low wavelet central frequency f_c , whereas the bandwidth parameter f_b value can be selected either small in the case of a low analyzed frequency interval or large for high analyzed frequencies.

Fig. 9 shows the averaged wavelet coherence and wavelet coherence ridges of the pressures at the chordwise pressure tap positions Nos. 3, 5, 7, 9 on the $B/D=1:1$ prism, the $B/D=1$ prism with SP and Nos. 3, 7, 11, 15 on the $B/D=5:1$ prism, at the spanwise positions $y=0$ and $y=25$ mm.

It is observed on the $B/D=1:1$ that the averaged wavelet coherences, by varying chord-wise pressure separation, tend to exclusively differ at very low frequencies, whereas the curves do not significantly change at higher frequencies (see Fig. 9(a)). Similar tendency can be seen in the

averaged wavelet coherences among the various chordwise pressure positions on the $B/D=1:1$ prism with SP (Fig. 9(b)).

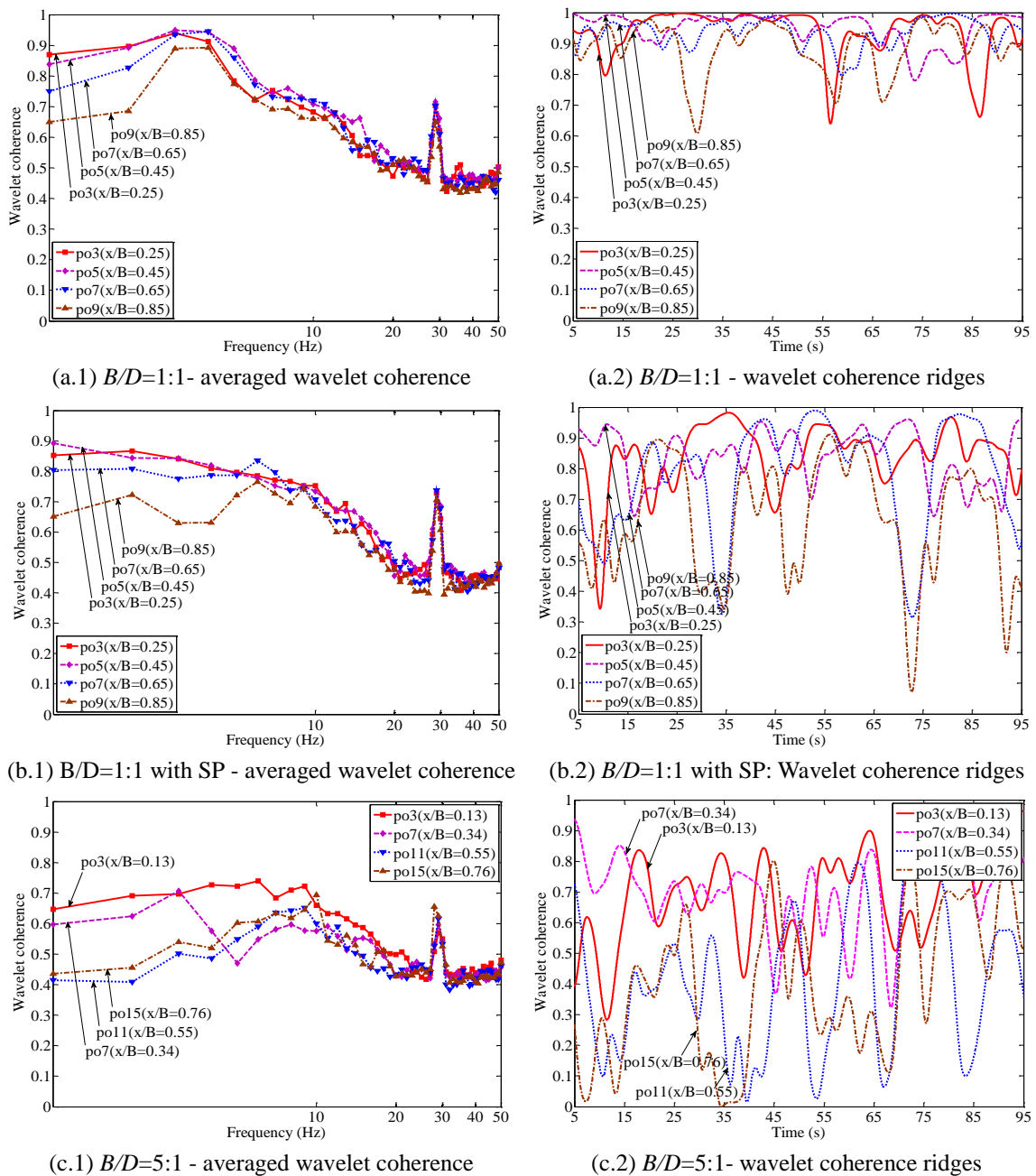


Fig. 9 Averaged wavelet coherence and wavelet coherence ridge of the pressure coefficients at various chordwise positions with $y=25\text{mm}$: (a) $B/D=1:1$, (b) $B/D=1:1$ with SP, (c) $B/D=5:1$

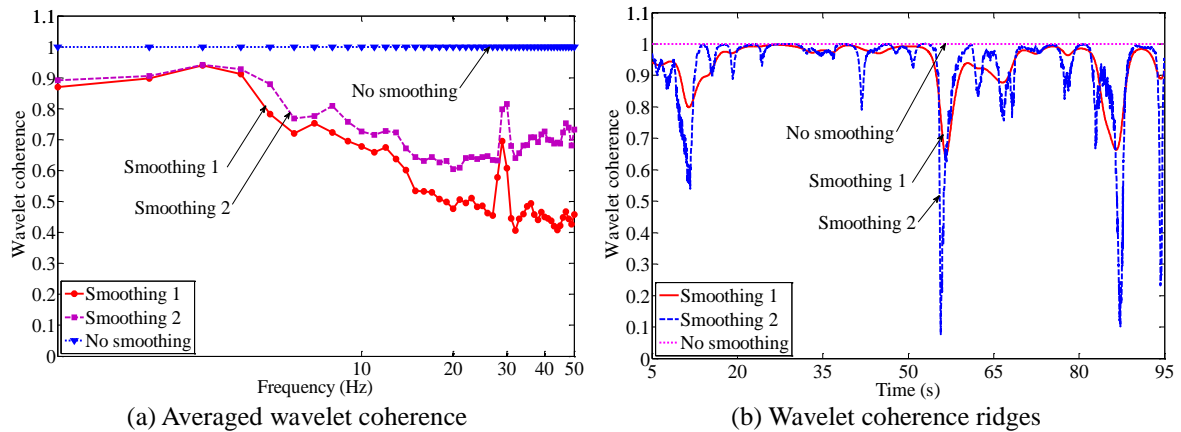


Fig. 10 Effect of time-scale smoothing ($B/D=1:1$, $y=25\text{mm}$) on: (a) Averaged wavelet coherence, (b) Wavelet coherence ridge

In the prism with $B/D=5:1$, there is significant difference in the wavelet coherences at the various chord-wise pressure positions (or separations), noticeable along the entire frequency axis. Generally, the averaged wavelet coherences of the pressures are high at the tap positions near the leading edge (positions Nos. 3, 5). The coherence reduces when the position indices move downstream, from the leading edge to the trailing edge (positions Nos. 7, 9 on the $B/D=1$ and Nos. 11, 15 on the $B/D=5$). This tendency is especially clear in the case of the $B/D=1:1$ prism and the $B/D=1:1$ prism with SP (see Fig. 11). This aspect may be explained due to a more uniform flow around the bluff body on the entire surface of the prism with $B/D=1:1$. In the prism with $B/D=5:1$, large averaged wavelet coherences are predominantly observed at the leading edge position No.3; they vary in a more complicated manner at the position No.7, near the reattachment region of the flow; also, a sudden reduction is also noted towards the trailing edge taps Nos. 11, 15 (Fig. 9(c)).

In the pressure coherence on the $B/D=5:1$, the wavelet coherence is relatively dominant around the leading edge positions within “the separation bubble” and progressively reduces at the reattachment region positions towards the trailing edge. Furthermore, the time-dependent coherence at the various chordwise pressure positions has been investigated by the wavelet coherence ridges. With the pressure positions moving downwind from the leading edge to the trailing edge of the prisms, the study of the wavelet coherence ridges suggests that low coherence events are characterized by an increment of their drops and an expansion of their duration along the time axis (see Fig. 9).

Fig. 10 illustrates the effect of the time-scale smoothing on the wavelet coherence of pressure on $B/D=1:1$ at the spanwise separation $y=25\text{ mm}$. Three cases of time-scale smoothing have been investigated: (i) time-averaged and weighted scale-averaged smoothing as presented in Section 3.5 (smoothing 1); (ii) localized time-averaged and scale-averaged smoothing (smoothing 2) and (iii) no smoothing on the time-scale plane. It is noted that the scale normalization has been used in all three cases. Furthermore, a localized 10-point adjacent region measured from each point on the time-scale plane has been employed for time-scale smoothing in the smoothing 2. In Fig. 10, there is a good agreement in the wavelet coherences between the smoothing 1 and the smoothing 2 at

low frequencies. However, non-negligible differences are observed with the increase of the frequencies in the high-frequency range. It is noted that the localized time-averaged and scale-averaged smoothing technique does not work well in estimating the wavelet coherence at high frequencies. If no smoothing is applied, the wavelet coherences are identically one on the whole time-scale plane. The effect of the time-scale smoothing on the time-dependent coherence ridge is depicted in Fig. 10(b). Influence of the time-scale smoothing on the corresponding confidence levels of the estimated wavelet coherence is beyond the scope of this study and will be considered in a future investigation.

Fig. 11 illustrates the results of a preliminary investigation on the confidence intervals of the estimated wavelet spectrum and wavelet coherence. First, lag-1 autocorrelations of the AR1 model describing the original pressure signals have been estimated to obtain the background power spectra of the simulated red noises. Second, a total of 1000 Monte-Carlo realizations (pairs) of the red noises have been synthetically generated to compute the wavelet coherence and the confidence intervals (Grinsted *et al.* 2004). Figs. 11(a) and 11(b) illustrate examples of the simulated red noises and verification of the assumption of red-noise by comparing the AR1 model spectrum with the average power spectrum of the original pressures.

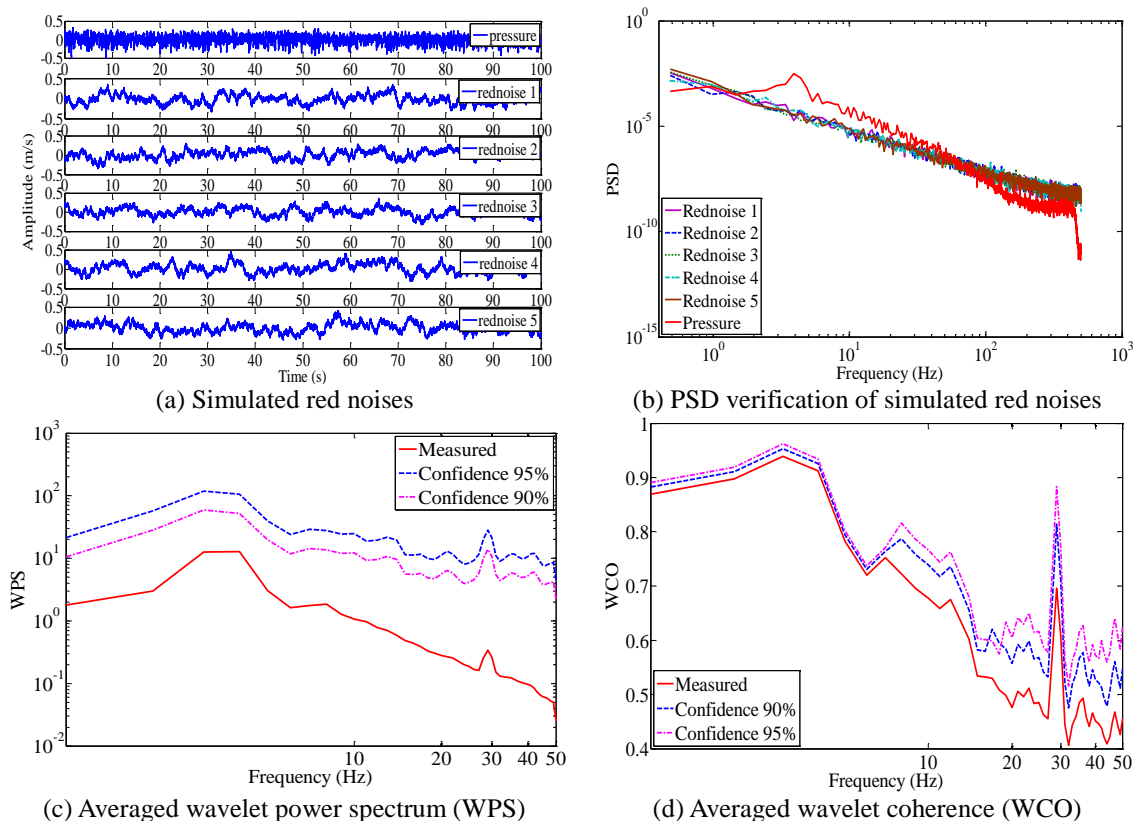


Fig. 11 Analysis of confidence intervals for wavelet spectrum and wavelet coherence ($B/D=1:1$, $y=25$ mm): (a) Simulated red noises, (b) PSD verification of the simulated red noises, (c) Averaged wavelet power spectrum (WPS), (d) Averaged wavelet coherence (WCO)

The wavelet coherences of the two synthetically generated pairs of red noises are finally employed to determine the confidence intervals (Figs. 11(c) and 11(d)). The selection of the confidence level (90% and 95%) and its effect on the estimation of the wavelet power spectrum and wavelet coherence are respectively illustrated in Figs. 11(c) and 11(d). As expected, the choice of significance level influences the confidence regions of the estimated wavelet spectra and wavelet coherences. The investigation suggests that any measured wavelet spectrum and wavelet coherence should be carefully interpreted and that analysis of confidence intervals should possibly be considered.

5. Conclusions

Wavelet coherence analysis has been employed to investigate the time-frequency coherence of wind turbulence and surface pressures, experimentally measured on the rectangular prisms in both spanwise and chordwise directions. The properties of modified complex Morlet wavelet function, normalization in scale, smoothing in time/scale and time-frequency resolution analysis have been considered in estimating the wavelet coherence. The averaged wavelet coherence and the wavelet coherence ridge have been proposed for better investigating the coherent structures of the wind turbulence and the surface pressures. The averaged wavelet coherence has also been verified with the Fourier coherence for the same sets of pressure data. The study has also examined the effects of fundamental flows, convection flows and turbulent conditions on the time-frequency coherence. The main remarks can be summarized as:

- (1) Scale normalization and time-scaling smoothing should be employed for the accurate estimation of the time-frequency coherence.
- (2) Time-frequency resolution significantly influences the wavelet pressure coherence; thus time-frequency resolution analysis must be carefully considered in computing the wavelet pressure coherence. It is suggested to select a low wavelet central frequency and adjustable bandwidth parameter in the modified Morlet wavelet function to obtain the desired resolution analysis.
- (3) Time-frequency coherence of the surface pressures depends on the flows in the proximity of the surface and in the wake of the prisms. The coherent structures of the pressures are strongly influenced by the dominant physical phenomena on the prisms (e.g., vortex shedding, separation bubble and flow reattachment).
- (4) Wavelet coherence ridge can be used to investigate the intermittent pressure features and intermittent rate of the time-frequency coherence in the time domain. Intermittent pressure features seem to exhibit a very similar behavior in the time domain at various spanwise separations.
- (5) Averaged wavelet coherence of the pressures generally agrees with the conventional Fourier coherence.
- (6) Coherent structures of the pressures are approximately similar in both spanwise and chordwise directions.
- (7) Time-scale smoothing, scale normalization and confidence interval analysis can significantly influence the numerical estimation and the interpretation of the estimated wavelet quantities.

Acknowledgements

Professors Masaru Matsumoto and Hiromichi Shirato from Kyoto University (Japan) are gratefully acknowledged for the technical assistance during the wind tunnel tests. The anonymous reviewers are acknowledged for providing insightful comments and useful observations.

References

- Bendat, J.S. and Piersol, A.G. (2000), *Random data: analysis and measurement procedures*, 3rd Ed., John Wiley and Sons.
- Bruno, L., Salvetti, M.V. and Ricciardelli, F. (2014), “Benchmark on the aerodynamics of a rectangular 5:1 cylinder: An overview after the first four years of activity”, *J. Wind Eng. Ind. Aerod.*, **126**, 87-106.
- Bruns, A. (2004), “Fourier-, Hilbert- and wavelet-based signal analysis: are they really different approaches?”, *Neuroscience Methods*, **137**, 321-332.
- Daubechies, I. (1992), *Ten lectures on wavelets*, Society of Industrial and Applied Mathematics, Philadelphia.
- Davenport, A.G. (1963), “The response of slender, line-like structures to a gusty wind”, *Proceedings of Institution of Civil Engineers*, **23**, 389-408.
- Geurts, C.P.W., Hajj, M.R. and Tieleman, H.W. (1998), “Continuous wavelet transform of wind and wind-induced pressures on a building in suburban terrain”, *Wind Eng. Ind. Aerod.*, **74-76**, 609-617.
- Grinsted, A., Moore, C. and Jevrejeva, S. (2004), “Application of the cross wavelet transform and wavelet coherence to geophysical time series”, *Nonlinear Proc. Geoph.*, **11**, 561-566
- Gurley, K., Kijewski, T. and Kareem, A. (2003), “First- and high-order correlation detection using wavelet transform”, *J. Eng. Mech. - ASCE*, **129**(2), 188-201.
- Jakobsen, J.B. (1997), “Span-wise structure of lift and overturning moment on a motionless bridge girder”, *J. Wind Eng. Ind. Aerod.*, **69-71**, 795-805.
- Kareem, A. and Kijewski, T. (2002), “Time-frequency analysis of wind effects on structures”, *Wind Eng. Ind. Aerod.*, **90**, 1435-1452.
- Kijewski, T. and Kareem, A. (2002), “On the presence of end effects and their melioration in wavelet-based analysis”, *J. Sound Vib.*, **256** (5), 980-988.
- Kijewski, T. and Kareem, A. (2003), “Wavelet transform for system identification in civil engineering”, *Comput. - Aided Civil. Infrastruct. Eng.*, **18**, 339-355.
- Krenk, S. (1996), “Wind field coherence and dynamic wind forces”, IUTAM Symposium on “Advances in nonlinear stochastic mechanics”, (Eds. Naess, A. and Krenk, S.), Kluwer Academic Publishers, Netherlands.
- Ladies, J. and Gouttebroze, S. (2002), “Identification of modal parameters using wavelet transform”, *Int'l J. Mechanical Sci.*, **44**, 2263-2283.
- Larose, G.L. (1996), “The span-wise coherence of wind forces on streamlined bridge decks”, *Proceedings of the 3rd International Colloquium on Bluff Body Aerodynamics and Applications (BBAA3)*, Blacksburg, USA.
- Le, T.H., Matsumoto, M. and Hiromichi, H. (2009), “Spanwise coherent structure of wind turbulence and induced pressure on rectangular cylinders”, *Wind Struct.*, **12**(5), 441-455.
- Le, T.H., Tamura, Y. and Matsumoto, M. (2011), “Spanwise pressure coherence on prisms using wavelet transform and spectral proper orthogonal decomposition based tools”, *Wind Eng. Ind. Aerod.*, **99**, 499-508.
- Liu, P.C. (1994), “Wavelet spectrum analysis and ocean wind waves”, *Wavelets in Geophysics*, (Eds. Foufoula-Georgiou, E. and Kumar, P.), Academic Press.
- Matsumoto, M., Shirato, H., Araki, K., Haramura, T. and Hashimoto, T. (2003), “Spanwise coherence characteristics of surface pressure field on 2-D bluff bodies”, *J. Wind Eng. Ind. Aerod.*, **91**, 155-163.

- Staszewski, W.J. (1998), "Identification of non-linear systems using multi-scale ridges and skeletons of the wavelet transform", *J. Sound Vib.*, **214**(4), 639-658.
- Simonovski, I and Boltežar, M. (2003), "The norms and variances of the Gabor, Morlet and general harmonic wavelet functions", *J. Sound Vib.*, **264**(3), 545-557.
- Torrence, C. and Compo, G.P. (1998), "A practical guide to wavelet analysis", *B. Am. Meteorol. Soc.*, **79**(1), 61-78.
- Yan, B.F., Miyamoto, A. and Bruhwiler, E. (2006), "Wavelet transform-based modal parameter identification considering uncertainty", *J. Sound Vib.*, **291**, 285-301.
- Zhan, Y., Halliday, D., Jiang, P., Liu, X. and Feng, J. (2006), "Detecting time-dependent coherence between non-stationary electrophysiological signals – A combined statistical and time-frequency approach", *Neuroscience Methods*, **156**, 322-332.